GPS Denied Localization and Magnetometer-Free Yaw Estimation for Multi-rotor UAVs

Naveen Balaji[1] Mangal Kothari[1] Abhishek Abhishek[1]

***Abstract*— This paper presents a range-based localization scheme for multi-rotor systems in GPS denied environments and proposes a novel methodology to estimate yaw attitude. The attitude and position are estimated using accelerometer, gyroscope, and range information with Extended Information Filter (EIF). The heading estimation is incorporated without the aid of magnetic sensors. All family of Gaussian filters requires the correct noise parameters for convergence and accurate estimation. We use an optimization technique for tuning the estimator's parameter (covariance matrices). Particle-Swarm Optimization (PSO) method is used for tuning the noise (covariance matrices) in the filter with the aid of ground truth in the initial flight. The effectiveness of tuned EIF is validated on the quadcopter platform with different environments, which shows superior performance compared to the manually tunned noise parameter.**

I. Introduction

Autonomous aerial systems capable of sensing and perceiving the environment have been the area of intense research due to their limitless applications, ranging from surveillance, precision agriculture, infrastructure inspection, photography, recreation etc. Unmanned Aerial Systems (UAS), such as quadcopters and unmanned helicopters, offer robust maneuverability with vertical takeoff and hovering capabilities on the three-dimensional airspace. They can perform tracking [1], inspections [2], and transportation [3] more quickly, economically, and safely compared to other comparable robots. The deployment of sophisticated sensors is incrementally enhancing intelligence of these aerial robots [4], enabling them to achieve autonomous navigation in complex and confined environments. The applications related to inspection and surveillance of commercial installations require these UAS to operate in GPS shadow areas where GPS signal reception may be diminished and less reliable. Further, the reliance of magnetometer for heading estimate is severely compromised if the UAS has to operate near large iron structures such as large cranes due to magnetic deviation.

Indoor Positioning System (IPS) becomes critical for many autonomous operations requiring application of UAS in GPS denied environments. Visual odometry for mobile robotics using feature tracking based on monocular and stereo-vision has been an active area of research to address indoor localization [5]–[7]. However, the solutions are sensitive to ambient lighting conditions, motion blur, and other artifacts that deteriorate image quality. Visual-inertial methods improved localization precision by eliminating scale factor error in the image with the fusion of inertial measurement unit (IMU) data [8]. The accumulation of drift in these methods are typical over time, thus cannot be used for long duration flights. Other SLAM based approaches popular among ground robots either use RGB-D cameras [9] or 3D lidars [10]. However, these approaches are often computationally expensive and time-intensive. They typically require onboard GPU computing ability to process data in real-time, which increases the power requirements and the overall weight of the system, thereby further compromising the endurance of aerial vehicle.

The wireless localization system, such as Radio Frequency Identification (RFID) [11], Wi-Fi [12], Zigbee [13] and Ultra-Wideband (UWB) [14], are emerging technologies for indoor localization solutions. Due to the unsatisfied accuracy of the received signal strength (RSS) techniques [15], they have not been found suitable for UAVs. Recently, UWB based technologies have gained momentum in this field. With the large bandwidth, this signal has the properties of strong multi-path resistance, which enables accurate ranging via communication by the two-way time of flight. They are low-cost, low-power, portable, robust and easy to implement in any environment.

The present work is an extension of the approach followed in [16], which focused on developing a pose estimation framework for quadcopter relying on MARG (inertial) sensor array, an optical flow camera, and a single Ultra-wideband (UWB) range sensor to correct the drift of the estimator over time. In this paper, use of multiple UWB sensors is proposed along with inertial sensors without any optical cameras for localization. Although some earlier research has focused on implementing Maximum likelihood based state estimation using UWB sensors [17], [18], it did not focus on optimizing the performance. The method used in this research aims to reduce the complexity of the algorithm using the extended information filter. Gaussian filters require a model of the system, comprising of a state function, measurement function, and the associated noise terms. The noise terms related to it are often difficult to estimate. The inaccurate noise model can cause perturbation in the estimation, which will lead to divergence of the filter. There are optimal ways to adapt a filter according to the need [19]. Noise covariance can be estimated by minimizing the cost function, with the known ground truth of the vehicle. In this paper, various criteria for tuning the filter are discussed, and the Particle Swarm Optimization (PSO) is employed for determining the best noise covariance.

[1]The authors are with the Department of Aerospace Engineering, Indian Institute of Technology Kanpur, Kanpur 208016, India. (e-mail: naveenb@iitk.ac.in, mangal@iitk.ac.in, abhish@iitk.ac.in)

Real-time tracking of the heading angle in rigid bodies has wide applications in robotics fields [20]. Inertial and magnetic sensor modules with their associated data filtering algorithms are designed for estimating attitude of the objects [21]. The famous estimation algorithms such as [22], allows accurate evaluation of pitch and roll attitude but are not robust for yaw estimations over time. The sources of magnetic interference are always present in common items such as current-conducting wires, batteries, and ferrous materials. Today there are many hybrid solutions such as [23], with expensive multiple sensors, to be used in the industrial environment for the estimation of the heading. This paper proposes to solve the problem of yaw estimation through a novel low-cost yaw estimation method without drift which can be used on UAS as fail-safe in the event of deterioration in yaw estimates from conventional MEMS magnetometers.

The remainder of the paper is structured as follows: the background work and problem statement is summarized in Sec. II. The localization and heading algorithms are given in Sec. III. The method of tuning the noise parameters based on PSO is given in Sec. IV. The experimental results and discussion are provided in Sec. V and concluding remarks are given in Sec. VI.

II. BACKGROUND AND PROBLEM STATEMENT

A. Problem Statement

The primary aim of this work is to localize an aerial vehicle (quadcopter) using IMU and UWB sensors. The UWB sensors are arranged at the corners of a rectangle to maintain a line-of-sight to the quadcopter as shown in Fig. 1. The current work uses a 3-axis MEMS accelerometer, a 3-axis MEMS gyroscope, and a 3-axis MEMS magnetometer as the inertial sensors equipped in the flight controller, which is a low-cost Invensense MPU6000 series. For magnetometer-free yaw estimation, measurements from magnetometer are discarded and another set of position measurement is used using another UWB sensor, the details are given in the next section. Bias in both acceleration and angular velocity is considered and explicitly estimated. All these sensors provide information on their local body frame. Due to the inconsistency of built-in barometer in the flight controller, a one-dimensional lidar in also incorporated to measure the altitude of the vehicle accurately. The ground truth reference is obtained using an eight camera Vicon motion capture system in indoor that provides precise estimates at 100 Hz [24].

B. Ultra-Wide Band Sensors

UWB sensor is a wireless sensor that transmit signals at 3-8 (GHz) bandwidth, offers high accuracy of signal with low power. It can measure distance through Time of Flight (ToF) of the radio signal, providing measurement range up to 100 m. The commercial-off-the-shelf UWB product Decawave DWM1001 [25] modules are used for the implementation of methodology proposed in the current paper. DWM1001 module has two modes: anchor mode (sending signal) and tag mode (receiving signal). The modules provides real-time

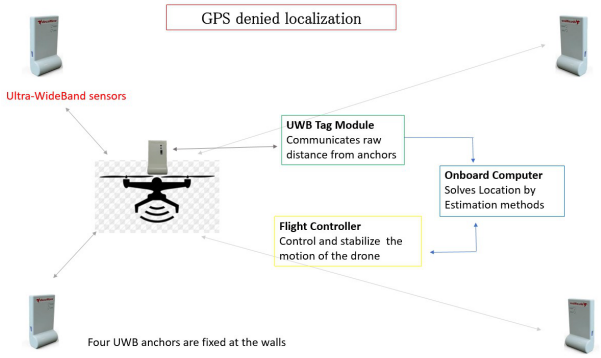

Fig. 1: The UWB sensors based localization architecture

location by the two-way ranging method. Then repeated reply algorithm is used to measure the time of flight between a tag and an anchor module. The time of flight can be estimated by subtracting the tag sensor processing time from the measured round-trip time of the signal sent by the tag to the anchor. The detail explanation of range estimation using two-way ranging method is available in [17], [26].

III. LOCALIZATION AND YAW ESTIMATION

In this section, a localization problem using UWB sensors is considered. The suite of UWB sensors acts as GPS and is integrated with IMU to provide accurate localization. Let P_A, P_B, P_B, P_D be the position of fixed anchors, as shown in Fig. 2, with respect to the inertial frame of reference. Let $P = (p_x, p_y, p_z)$ be the vehicle co-ordinate that need to be estimated by a localization algorithm when provide with distances d_1, d_2, d_3, and d_4 as follows:

$$(P-P_A)^2 = d_1^2;\ (P-P_B)^2 = d_2^2;\ (P-P_C)^2 = d_3^2;\ (P-P_D)^2 = d_4^2;$$

The above set of equations can be solved either using nonlinear least square (NLS) method or using a (Bayesian and/or Gaussian) filter. As known the solution of NLS is corrupted with noise, therefore the filter based method is employed in this work. Extended Information Filter (EIF) is used due to its ease of implementation and time complexity.

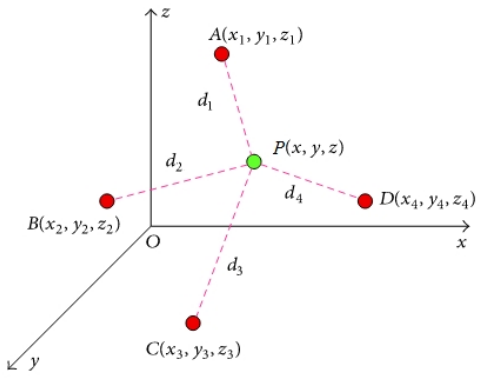

Fig. 2: Point form of the problem statement

A. Extended Information Filter

The EIF [27] is an algebraic equivalent of the EKF in which Gaussian is parametrized by information vector, ξ, and information matrix, Ω, rather than the mean and covariance. For the fusion of multiple UWB sensors, EIF is preferred over EKF, due to its simplicity in measurement step. The prediction and update steps of EIF for localization are described below:

Prediction Step

The inertial sensor, accelerometer and gyroscope data is used for prediction. A constant acceleration model is considered for prediction step with acceleration bias, $a_b = [a_{bx},\ a_{by},\ a_{bz}]$. The state transition model is given as follows:

$$p_k = p_{k-1} + v_k\ T + \frac{a_k\ T^2}{2} - \frac{a_{bk}\ T^2}{2} \tag{1}$$

where p is the position vector, v is the velocity, the acceleration vector given by

$$a_k = \mathcal{R}_k\ \vec{a_{kbody}} + \vec{g}$$

at k^{th} time step, and T is time interval taken for integration. Here $\mathcal{R}_k$ is a rotation matrix from the body to inertial frames. The state vector for localization and bias estimation is defined as

$$X = [p_x\ , v_x,\ a_{bx}\ , p_y\ , v_y\ , a_{by}\ , p_z\ , v_z\ , a_{bz}\ ]^T$$

Having defined this, the information vector and matrix are given as follows:

$$\xi_k = \Sigma_k^{-1}\ x_k \qquad\qquad \Omega_k = \Sigma_k^{-1} \tag{2}$$

where Σ_k is the covariance matrix at time step k. The prediction steps are given as

$$\hat{\xi}_k \quad = \quad \hat{\Omega}_k\ \left(F_k\ \Omega_{k-1}^{-1}\ F_k^T + G_k\ u_k\right) \tag{3}$$

$$\hat{\Omega}_k \quad = \quad \left(\ F_k\ \Omega_{k-1}^{-1}\ F_k^T + Q_k\right)^{-1} \tag{4}$$

where $u_k = [\ a_{x_k},\ 0,\ 0,\ a_{y_k},\ 0,\ 0,\ a_k,\ 0,\ 0\ ]^T$ and

$$F_k = \begin{bmatrix} F_k^{'} & 0 & 0 \\ 0 & F_k^{'} & 0 \\ 0 & 0 & F_k^{'} \end{bmatrix},\ F_k^{'} = \begin{bmatrix} 1 & T & \frac{-T^2}{2} \\ 0 & 1 & -T \\ 0 & 0 & 1 \end{bmatrix}$$

$$G_k = \begin{bmatrix} G_k^{'} & 0 & 0 \\ 0 & G_k^{'} & 0 \\ 0 & 0 & G_k^{'} \end{bmatrix},\ G_k^{'} = \begin{bmatrix} \frac{-T^2}{2} & 0 & 0 \\ T & 0 & 0 \\ 0 & 0 & 0 \end{bmatrix}$$

where Q_k is the process noise. The process noise matrix is ideally modeled, in order to obtain the Markov property, which is required in recursive Bayesian inference. It is assumed that Q_k is a function of a single variable (τ_a for a_{world} and τ_b for a_{bias}) which is approximated to be constant over time [28]. The continuous time zero-mean white noise modeled with bias superposition for the system is:

$$Q_k^{'} = \begin{bmatrix} \frac{T^3\tau_a}{3} + \frac{T^5\tau_b}{20} & \frac{T^2\tau_a}{2} + \frac{T^4\tau_b}{8} & -\frac{T^3\tau_b}{6} \\ \frac{T^2\tau_a}{2} + \frac{T^4\tau_b}{8} & T^2\tau_a + \frac{T^3\tau_b}{3} & -\frac{T^2\tau_b}{2} \\ -\frac{T^3\tau_b}{6} & -\frac{T^2\tau_b}{2} & -T^3\tau_b \end{bmatrix}$$

UWB Measurement Update

The range measurements obtained from the UWB senors for the update equation is

$$r_k = \left[\sqrt{(p_x - p_{Ax})^2 + (p_y - p_{Ay})^2 + (p_z - p_{Az})^2}\ \right]$$

where (p_{Ax}, p_{Ay}, p_{Az}) are the known position of anchor modules. The measurement update is carried out as following

$$\xi_k \quad = \quad \hat{\xi_k} + H_k^T R_k^{-1}[r_k - h(\hat{x}_k) + H_k\ \hat{x}_k] \tag{5}$$

$$\Omega_k \quad = \quad \hat{\Omega}_k + H_k^T R_k^{-1} H_k \tag{6}$$

where h_k is the measurement model given by r_k, $h(\hat{x}_k)$ is computed at $\hat{x}_k$,

$$H_k = \frac{\partial h}{\partial x_k} = \left[\frac{p_x - p_{Ax}}{\bar{r}_k}, 0, 0, \frac{p_x - p_{Ay}}{\bar{r}_k}, 0, 0, \frac{p_x - p_{Az}}{\bar{r}_k}\right]^T$$

In the above equation, R_k is measurement noise. In addition to this, the median filter ise used to remove the outliers of UWB readings that will result in a sudden change of the estimated position. The difference between the predicted distance $h(\hat{x}_k)$ and the actual UWB measurements r_k as $d_k = |h(\hat{x}_k) - r_k|$ is calculated and if the error term is over a certain threshold, the measurement is discarded.

Height Measurement Update

The altitude measurement z_k obtained from the 1D lidar data l_k rotated to inertial frame for update step is

$$z_k = \ l_k R_k[3,3]\ = l_k \cos\theta \cos\phi$$

where θ and ϕ are pitch and roll angles. The measurement matrix for updating height $[z_k]$ is

$$H_k = [\ 0,\ 0,\ 0,\ 0,\ 0,\ 0,\ 1,\ 0,\ 0\ ]$$

The information vector and matrices are updated using (5) and (6).

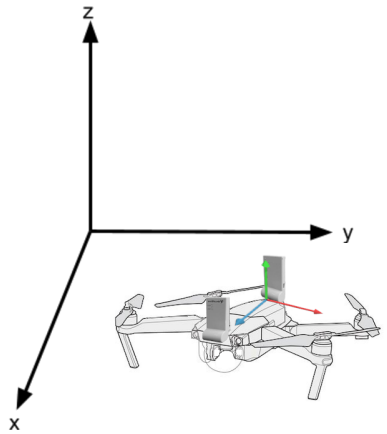

Fig. 3: Yaw Estimation in fixed inertial frame

B. Yaw Estimation

For the yaw estimation, the UAS system is enhanced by mounting two UWB sensors on the quadcopter along with MARG sensors, as shown in Fig. 3. In order to determine yaw, the position of two tag sensors p_1, p_2 are estimated using the similar approach described above. The modified state vector is given as

$$\mathbf{X} = [p_{x1}, p_{x2}, v_x, a_{bx}, p_{y1}, p_{y2}, v_y, a_{by}, p_{z1}, p_{z2}, v_z, a_{bz}, \psi]^T$$

Using these position, the yaw measurement is computed as

$$\psi = \cos^{-1}\left(\frac{p_{x2} - p_{x1}}{d_k}\right)$$

where

$$d_k = \sqrt{(p_{x2} - p_{x1})^2 + (p_{y2} - p_{y1})^2 + (p_{z2} - p_{z1})^2}$$

The control vector, u, now has a extra input, ω, about the fixed inertial frame z-axis. The dynamics is the same as described in the previous section. The Jacobin computed for this update step is the

$$H_k = [\ \frac{\sqrt{{d_k}^2 - (p_{x2} - p_{x1})^2}}{{d_k}^2}, -\frac{\sqrt{{d_k}^2 - (p_{x2} - p_{x1})^2}}{{d_k}^2}, 0, 0,$$

$$-\frac{(p_{y2} - p_{y1}).(p_{x2} - p_{x1})}{{d_k}^2.\sqrt{{d_k}^2 - (p_{x2} - p_{x1})^2}}, \frac{(p_{y2} - p_{y1}).(p_{x2} - p_{x1})}{{d_k}^2.\sqrt{{d_k}^2 - (p_{x2} - p_{x1})^2}}, 0, 0,$$

$$-\frac{(p_{z2} - p_{z1}).(p_{x2} - p_{x1})}{{d_k}^2.\sqrt{{d_k}^2 - (p_{z2} - p_{x1})^2}}, \frac{(p_{z2} - p_1).(p_{x2} - p_{x1})}{{d_k}^2.\sqrt{{d_k}^2 - (p_{x2} - p_{x1})^2}}, 0, 0, 1\ ]^T$$

Each UWB sensor provides data at 10 Hz. The 1D lidar data is obtained at 20 Hz. The processed IMU data is collected about 80-100 Hz. The full state estimation of the quadcopter is carried at 50 Hz.

IV. Optimization of Noise Parameters

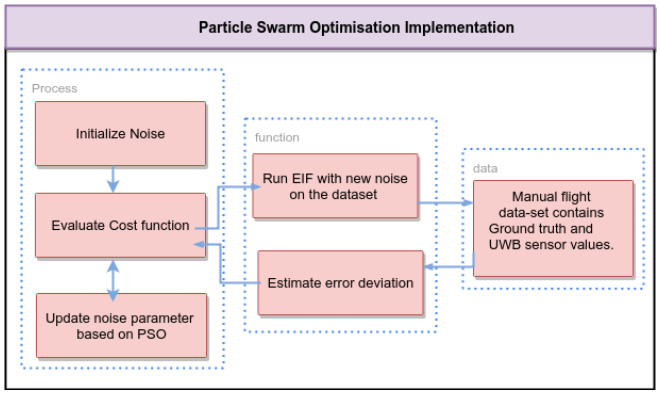

Fig. 4: Architecture of filter tuning

This section discusses a way to choose optimize noise parameters of EIF implemented in the previous section. For simplicity, the discussion focuses on optimally choosing state-model and sensor noises, assuming that the dynamics considerations in vehicle state-model equations are perfect. Due to the directional nature of UWB sensor antenna, the noise given by the manufacturer and statically estimated was not effective for robots EIF. Abbeel and Thrun [29] have discussed various methods to train the noise parameter for Kalman filter. In this work, the minimization of residual prediction error is considered. The prediction error minimization technique seeks the sensor noise (R) and system noise (Q) in a implicit manner. Then the noise parameters minimize the quadratic deviation of (z) (ground truth) and its corresponding expected state vector (ν) , weighted by information matrix (Ω).

$$< Q_{res}, R_{res} > = arg\min_{R,Q} \sum_{t=0}^{N} (z_t - \nu_t)\Omega_t(z_t - \nu_t)^T \quad (7)$$

where N is the total number of steps and t is the time step considered for training data.

A. PSO implementation

Algorithm 1 PSO implementation

CostFunction (particle$_i$)
1: (τ_a, τ_b, R) = particle$_i$.pose
2: Evaluate(residual prediction error) {with τ_a, τ_b, R}
3: return error

Velocity (particle$_i$)
1: vel_cognitive = c_1(particle$_i$.pose_best − particle$_i$.position)
2: vel_social = c_2 (global_best_pose − particle$_i$.position)
3: vel$_{k+1}$ = c_3.particle$_i$.vel$_k$ + vel_cognitive + vel_social
4: return vel$_{k+1}$

Main ( )
1: number of particles =10
2: Initialize all 10 particles with (τ_a, τ_b, R)
3: max_iteration = 30
4: **for** i in max_iteration **do**
5: **for** j in number of particles **do**
6: Costfunction(particle$_j$)
7: **if** particle$_j$.error < particle$_j$.min_error **then**
8: particle$_j$.pose_best = particle$_j$.pose
9: particle$_j$.min_error = particle$_j$.error
10: **end if**
11: **if** particle$_j$.error < global_min_error **then**
12: global_best_pose = particle$_j$.pose
13: global_min_error = particle$_j$.error
14: **end if**
15: **end for**
16: **for** j in number of particles **do**
17: particle$_j$.pose = particle$_j$.pose+Velocity(particle$_j$)
18: **end for**
19: **end for**
20: return(global_best_pose)

Particle Swarm Optimization (PSO) algorithm is used to determine the optimum noise parameters corresponding to minimum residual prediction error. The PSO is a heuristic

method [30], derived from the concept of swarming habits of animals such as birds or fish and have been useful for solving nonlinear optimization problems. In the tuning process, the filter covariance matrices are estimated as follows. At first, the noise matrice is reduced as a function of single variable for simplicity, as described in eqn.III-A. The problem is posed as to find best fit system noise (τ_a), inertial system bias noise (τ_b), and UWB range noise (R) subject to eqn.(7).

The PSO algorithm maintains multiple optimal points in the search space at a time. Each optimal point is represented as a particle with noise parameters as its position (τ_a, τ_b, R). At each iteration, depending on function values search direction is formed and the position is updated. In Algorithm 1, the procedure of PSO algorithm is outlined. The algorithm return values (τ_a, τ_b, R) depends on the starting point and the hyperparameters (c_1, c_2, c_3). The algorithm initializes all the particle's 3D position randomly. Then the iterations starts from Line 4. First, the cost function is evaluated for all the particles with its position/noise parameter (τ_a, τ_b, R). The cost function in algorithm provides us the residual prediction error estimated by evaluation of collected dataset. For each iteration the particle's minimum, and the global minimum error are stored. Then the position of each of the particles is updated with the help of velocity term (Line 17). The velocity as shown in algorithm comprises of 3 terms as follows. The cognitive term, which emphasis search direction on the individual particle's best point evaluated. The social term makes the search direction towards the global best point evaluated. And the last term gives importance to the particle's previous position. The total velocity is governed by the weighted average of the mentioned three terms with the hyperparameters (c_1, c_2, c_3). The next iteration starts with the particle's updated position and continues till the max iterations. The weights (c_1, c_2, c_3) constraints the searching time and space. Here, the (c_1, c_2, c_3) are chosen for the convergence of the function rather than exploring the search space vastly. The sketch of PSO implementation is given in Fig. 4. After a certain number of iterations, the algorithm is expected to converge to the optimum parameters. Although the number of particles and iterations are fixed for our experiment in Algorithm 1, one can choose these values based on the experiment setup.

V. Experimentation Results

1) Experimental setup information: A series of experiments were conducted both in the indoor lab setup and in the outdoor environments to evaluate the accuracy of our position and attitude estimator on a quadcopter model. The tuning of covariance is performed offline using the optimization method described in the previous section. The training data set is collected using the motion capture system as the ground truth, along with other sensors data. Then the experiments are conducted with optimized noise parameters. We first analyze the result of PSO-tuned EIF in indoor environment and in the second part we validate the same noise parameters for outdoor experiments .

The multicopter position controller in autopilot (PixHawk) is initially tuned with the motion capture system [31]. A Raspberry Pi 3 running Ubuntu mate is used as an onboard computer. Robot Operating System (ROS) environment is used for implementing the state estimator. This EIF then communicates with the flight controller to provide high-level position and heading commands via the mavlink protocol. The quadcopter generally provide their local orientations and acceleration with respect to ENU (East-North-Up) frame. Since the UWB anchors used in the current study are fixed up in a different direction, the UWB position estimates need to be transformed to the ENU frame by rotating with the yaw offset before sending this data to the flight controller. The UWB anchors were placed at the corners of 10×10m square of height of around 2m in the environment.

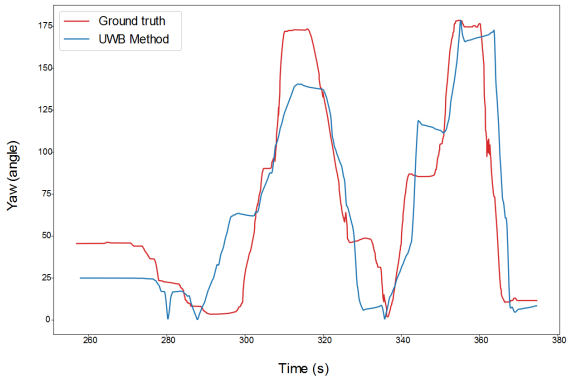

Fig. 5: Accuracy of yaw estimation

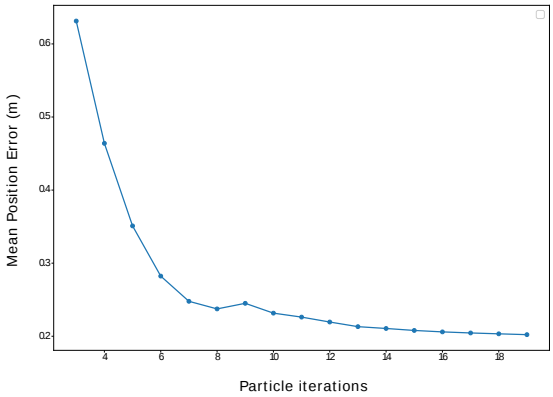

Fig. 6: Convergence of cost function error in PSO algorithm

2) Attitude accuracy: The roll and pitch attitude estimation is estimated by Pixhawk stack [31]. The heading angle estimated from Pixhwak stack suffered from deflection in the indoor environment due to interface with magnetic fields. Two UWB's system, as described in the previous section, were placed on quadrotor for yaw estimation. Our solution for yaw estimation has no external magnetic deflections

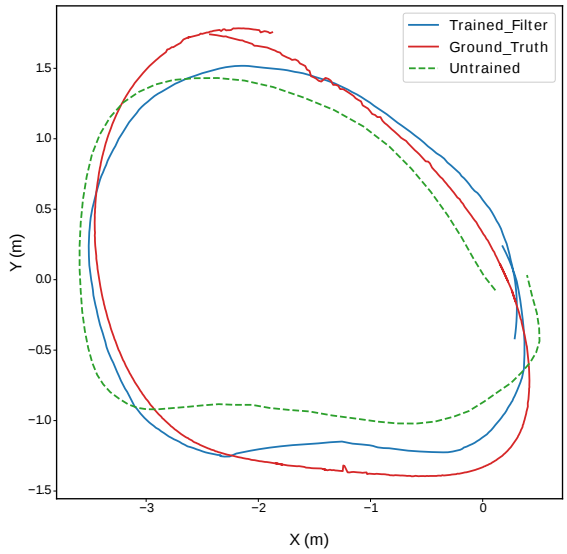

(a) Trajectory of state estimator in x-y plane

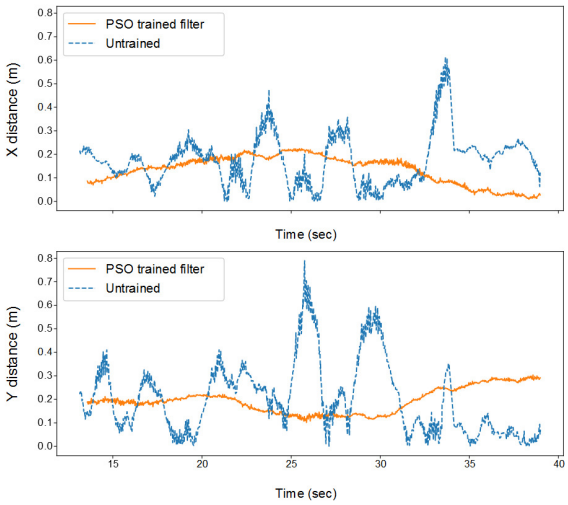

(b) Position error in x and y directions

Fig. 7: Indoor localization of the quadcopter

and no drift over time. The gyroscope data about 100Hz frequency was integrated to estimated attitude. In the indoor experiment we gave a rotational yaw moment in manual control mode as shown in Fig. 5. It can be seen from the figure UWB method is comparable with the ground truth. Hence, the proposed approach is able to estimate yaw attitude quite accurately.

3) Training accuracy: The hand-tuned filter noise fit well in some instances but when the aggressive maneuvers are performed, the filter sensitivity is inadequate. The optimization method of determining covariance with the training data is a quick process and results in precise results. The PSO algorithm valuated with weight $c_1 = 1$, $c_2 = 1$, $c_3 = 0.55$ converged within 30 iterations and provided us the noise parameters $\tau_a = 0.151$, $\tau_b = 1.37$ and $R = 0.18$. The RMS error with iterations are shown in Fig. 6 and it can be seen that the position error converges to a smaller value. This accuracy shows that the autonomous navigation of quadrotor is possible with help of localization with UWB sensor suite.

4) Position estimation accuracy: Initially, the experiment is conducted in an indoor environment using a single UWB receiver (tag) placed on the quadcopter for position estimation. The quadrotor is asked to follow a circular trajectory as shown in Fig. 7(a). It can be seen from the figure that the PSO tunned approach gives better results compared to hand tunned method. The PSO tunned method accurately localize the quadrotor within the error range of 0.2m when compared to ground truth values. The use of 1-D lidar in experiments have helped in achieving accurate estimation as compared to inbuilt barometer data. The z RMS error for the localization comes out to be 0.048m. The RMS error for PSO and hand tunned methods is tabulated in Table 1. Although the error are of the same order, the PSO tunned approach provides better accuracy. Therefore, it can be concluded that the tunning using optimization method helps in achieving better accuracy. Next, the efficacy of tunning process is done in the outdoor environment.

TABLE I: Performance of Indoor Localization

Position Error	X axis	Y axis	Z axis	YAW
Untrained EIF	0.273m	0.257m	0.063m	0.28 (rad)
Trained EIF	0.166m	0.189m	0.048m	0.17 (rad)

5) Outdoor Test: In the outdoor environment, the PSO trained noise model is compared against the ground truth acquired through the RTK-GPS of about 2-5 cm accuracy [32]. The localization setup is same as used in the indoor experiment. For testing, the quadcopter was operated autonomous in a square trajectory. The estimated path for PSO tunned, hand tunned, and RTK GPS based approaches is shown in Fig. 8. It can be seen from the figure that the PSO tunned estimates are quite close to RTK GPS based estimates. The RMS error for PSO and hand tunned methods for the outdoor environment is tabulated in Table 2. It can be seen from the table that the PSO trained approach performs better compared to hand trained approach. This show that the tunned parameters are effective in the different environment as well. Hence, it can be concluded that the tunning is adequate.

TABLE II: Performance of Outdoor Localization

Position Error	X axis	Y axis	Z axis
Untrained EIF	0.243m	0.257m	0.116m
Trained EIF	0.146m	0.169m	0.092m

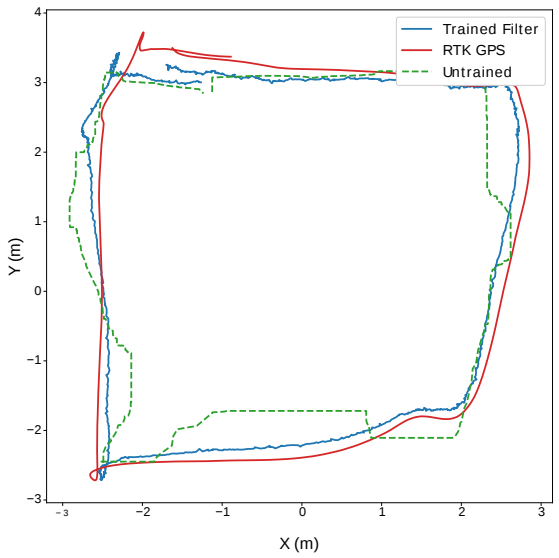

Fig. 8: Outdoor test results

VI. Conclusion

In this paper, a low-cost localization methodology has been presented for aerial vehicles using Extended Information Filter (EIF) with the range information. The noise parameters are optimally tunned using PSO algorithm with ground truth data. This approach have been tested in different environmental conditions with high accuracy. Experiments conducted both in the indoor and outdoor environment validated the approach. This suggests that our estimation model technique yields better results with less manual effort. The yaw estimates obtained are promising and can be used as a failsafe to revert to in case of large magnetic deviation in the conventional MEMS magnetometer. The proposed solution can be extended to coordinate multiple vehicles in GPS denied environments.

References

[1] J. Kim and Y. Kim, "Moving ground target tracking in dense obstacle areas using uavs," *IFAC Proceedings Volumes*, vol. 41, no. 2, pp. 8552–8557, 2008.

[2] N. Nigam, S. Bieniawski, I. Kroo, and J. Vian, "Control of multiple uavs for persistent surveillance: algorithm and flight test results," *IEEE Transactions on Control Systems Technology*, vol. 20, no. 5, pp. 1236–1251, 2011.

[3] A. Raptopoulos, D. Damm, M. Ling, and I. Baruchin, "Transportation using network of unmanned aerial vehicles," July 5 2016. US Patent 9,384,668.

[4] G. Cai, J. Dias, and L. Seneviratne, "A survey of small-scale unmanned aerial vehicles: Recent advances and future development trends," *Unmanned Systems*, vol. 2, no. 02, pp. 175–199, 2014.

[5] D. Scaramuzza and F. Fraundorfer, "Visual odometry [tutorial]," *IEEE robotics & automation magazine*, vol. 18, no. 4, pp. 80–92, 2011.

[6] M. Achtelik, M. Achtelik, S. Weiss, and R. Siegwart, "Onboard imu and monocular vision based control for mavs in unknown in-and outdoor environments," in *2011 IEEE International Conference on Robotics and Automation*, pp. 3056–3063, IEEE, 2011.

[7] M. Achtelik, A. Bachrach, R. He, S. Prentice, and N. Roy, "Stereo vision and laser odometry for autonomous helicopters in gps-denied indoor environments," in *Unmanned Systems Technology XI*, vol. 7332, p. 733219, International Society for Optics and Photonics, 2009.

[8] J. Delmerico and D. Scaramuzza, "A benchmark comparison of monocular visual-inertial odometry algorithms for flying robots," in *2018 IEEE International Conference on Robotics and Automation (ICRA)*, pp. 2502–2509, IEEE, 2018.

[9] C. Kerl, J. Sturm, and D. Cremers, "Dense visual slam for rgb-d cameras," in *2013 IEEE/RSJ International Conference on Intelligent Robots and Systems*, pp. 2100–2106, IEEE, 2013.

[10] Y. Xu, Y. Ou, and T. Xu, "Slam of robot based on the fusion of vision and lidar," in *2018 IEEE International Conference on Cyborg and Bionic Systems (CBS)*, pp. 121–126, IEEE, 2018.

[11] J. Zhou and J. Shi, "Rfid localization algorithms and applications—a review," *Journal of intelligent manufacturing*, vol. 20, no. 6, p. 695, 2009.

[12] A. Polo, F. Viani, E. Giarola, G. Oliveri, P. Rocca, and A. Massa, "Semantic wireless localization enabling advanced services in museums," in *The 8th European Conference on Antennas and Propagation (EuCAP 2014)*, pp. 443–446, IEEE, 2014.

[13] N. Watthanawisuth, A. Tuantranont, and T. Kerdcharoen, "Design of mobile robot for real world application in path planning using zigbee localization," in *2014 14th International Conference on Control, Automation and Systems (ICCAS 2014)*, pp. 1600–1603, IEEE, 2014.

[14] A. Alarifi, A. Al-Salman, M. Alsaleh, A. Alnafessah, S. Al-Hadhrami, M. Al-Ammar, and H. Al-Khalifa, "Ultra wideband indoor positioning technologies: Analysis and recent advances," *Sensors*, vol. 16, no. 5, p. 707, 2016.

[15] A. R. J. Ruiz, F. S. Granja, J. C. P. Honorato, and J. I. G. Rosas, "Accurate pedestrian indoor navigation by tightly coupling foot-mounted imu and rfid measurements," *IEEE Transactions on Instrumentation and measurement*, vol. 61, no. 1, pp. 178–189, 2011.

[16] K. S. Gaur, H. Parwana, A. Bhatt, G. Pandey, and M. Kothari, "Low cost solution for pose estimation of quadrotor," in *2018 AIAA Information Systems-AIAA Infotech@ Aerospace*, p. 0466, 2018.

[17] M. W. Mueller, M. Hamer, and R. D'Andrea, "Fusing ultra-wideband range measurements with accelerometers and rate gyroscopes for quadrocopter state estimation," in *2015 IEEE International Conference on Robotics and Automation (ICRA)*, pp. 1730–1736, IEEE, 2015.

[18] J. Li, Y. Bi, K. Li, K. Wang, F. Lin, and B. M. Chen, "Accurate 3d localization for mav swarms by uwb and imu fusion," in *2018 IEEE 14th International Conference on Control and Automation (ICCA)*, pp. 100–105, IEEE, 2018.

[19] Y. Yang and W. Gao, "An optimal adaptive kalman filter," *Journal of Geodesy*, vol. 80, no. 4, pp. 177–183, 2006.

[20] B. Barshan and H. F. Durrant-Whyte, "Inertial navigation systems for mobile robots," *IEEE Transactions on Robotics and Automation*, vol. 11, no. 3, pp. 328–342, 1995.

[21] R. Mahony, T. Hamel, and J.-M. Pflimlin, "Nonlinear complementary filters on the special orthogonal group," *IEEE Transactions on automatic control*, vol. 53, no. 5, pp. 1203–1217, 2008.

[22] S. Madgwick, "An efficient orientation filter for inertial and inertial/magnetic sensor arrays," *Report x-io and University of Bristol (UK)*, vol. 25, pp. 113–118, 2010.

[23] M. Bentley, "Wireless and visual hybrid motion capture system," Apr. 26 2016. US Patent 9,320,957.

[24] P. Merriaux, Y. Dupuis, R. Boutteau, P. Vasseur, and X. Savatier, "A study of vicon system positioning performance," *Sensors*, vol. 17, no. 7, p. 1591, 2017.

[25] "Decawave dwm1001 datasheet." `https://www.decawave.com/`. (Accessed on 10/09/2019).

[26] I. Dotlic, A. Connell, H. Ma, J. Clancy, and M. McLaughlin, "Angle of arrival estimation using decawave dw1000 integrated circuits," in *2017 14th Workshop on Positioning, Navigation and Communications (WPNC)*, pp. 1–6, IEEE, 2017.

[27] A. G. O. Mutambara and H. F. Durrant-Whyte, "Nonlinear information space: a practical basis for decentralization," in *Sensor Fusion VII* (P. S. Schenker, ed.), vol. 2355, pp. 97 – 105, International Society for Optics and Photonics, SPIE, 1994.

[28] R. Labbe, "Kalman and bayesian filters in python," 2015.

[29] P. Abbeel, A. Coates, M. Montemerlo, A. Y. Ng, and S. Thrun, "Discriminative training of kalman filters.," in *Robotics: Science and systems*, vol. 2, p. 1, 2005.

[30] J. Kennedy and R. Eberhart, "Particle swarm optimization," in *Proceedings of ICNN'95-International Conference on Neural Networks*, vol. 4, pp. 1942–1948, IEEE, 1995.

[31] "Multicopter autopilot." `https://docs.px4.io/`. (Accessed on 26/02/2020).

[32] T. Takasu and A. Yasuda, "Development of the low-cost rtk-gps receiver with an open source program package rtklib," in *International symposium on GPS/GNSS*, pp. 4–6, International Convention Center Jeju Korea, 2009.